Bulletin of the Seismological Society of America, Vol. 92, No. 4, pp. 1543–1560, May 2002

Comments on Baseline Correction of Digital Strong-Motion Data: Examples from the 1999 Hector Mine, California, Earthquake

by David M. Boore, Christopher D. Stephens, and William B. Joyner*

Abstract Residual displacements for large earthquakes can sometimes be determined from recordings on modern digital instruments, but baseline offsets of unknown origin make it difficult in many cases to do so. To recover the residual displacement, we suggest tailoring a correction scheme by studying the character of the velocity obtained by integration of zeroth-order-corrected acceleration and then seeing if the residual displacements are stable when the various parameters in the particular correction scheme are varied. For many seismological and engineering purposes, however, the residual displacements are of lesser importance than ground motions at periods less than about 20 sec. These ground motions are often recoverable with simple baseline correction and low-cut filtering. In this largely empirical study, we illustrate the consequences of various correction schemes, drawing primarily from digital recordings of the 1999 Hector Mine, California, earthquake. We show that with simple processing the displacement waveforms for this event are very similar for stations separated by as much as 20 km. We also show that a strong pulse on the transverse component was radiated from the Hector Mine earthquake and propagated with little distortion to distances exceeding 170 km; this pulse leads to large response spectral amplitudes around 10 sec.

Introduction

High-dynamic-range, broadband digital recordings of ground accelerations from earthquakes have the potential to yield ground displacements over a wide range of frequencies, including those so low that the displacements give the residual static deformation following an earthquake. These records are of great interest to seismologists for unraveling the complexities of fault rupture and may be of interest to engineers designing large structures with very long-period response. Unfortunately, accumulating experience indicates that the digital recordings are often plagued by what we call baseline offsets: small steps or distortions in the reference level of motion (Iwan *et al.*, 1985; Chiu, 1997; Boore, 1999, 2001). Although small in acceleration, these offsets can produce completely unrealistic ground displacements (derived from the acceleration traces by double integration). There may be numerous sources of the offsets (e.g., hysteresis in the sensor, static buildup in the A/D converter, or tilting of the ground), and for this reason, there is no universal correction scheme that can be applied blindly to the records. Ideally, the physical mechanisms causing the offsets would be known, so that a correction scheme could be tailored for each particular record. In most cases this is too time consuming when dealing with many records from a particular earthquake, or is impossible because of fundamental uncertainties in the source of the problems. In such cases, the very long period motions must be sacrificed, and a combination of baseline correction and low-cut filtering can be used to produce motions that are accurate representations of the true ground motions at periods of interest to engineers and to many earthquake modelers. In this article we describe and illustrate several simple processing schemes, including those that we are currently using at the U.S. Geological Survey (USGS). Our examples are primarily from the **M** 7.1 1999 Hector Mine earthquake (a map of the stations is given in Fig. 1; information about the recorders is given in the caption). We are concerned with corrections at low frequencies; the corrections at high-frequency, usually for instrument response, are generally not necessary with the force-balance accelerometers commonly used, at least for frequencies of usual seismological and engineering interest ($f < 20$ Hz).

Examples of Baseline Problems

An example of the problem is shown in Figure 2, using the recording of the 1999 Hector Mine earthquake from station HEC (this is the closest station to the epicenter and rupture surface). The top trace shows the recorded acceleration after subtracting the mean of the pre-event portion of the

*Deceased, 24 March 2001.

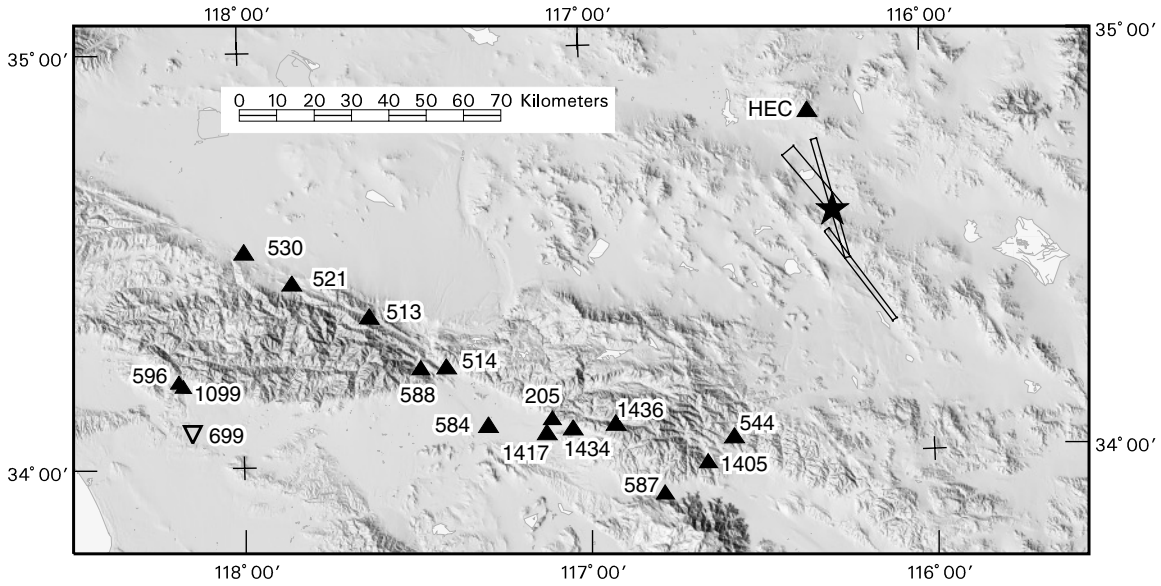

Figure 1. Map showing stations from which records used in this paper were obtained. Stations shown are only a small subset of all of the stations that recorded the earthquake (see *http://nsmp.wr.usgs.gov* and Graizer *et al.*, 2002). The record at Station 699 was obtained on the 12th floor of a 12-story building; all other stations are considered to be free-field recordings. The three rectangles near the epicenter are the surface projections of the fault planes used in Ji *et al.*'s (2002) fault model; the epicenter is shown by the star. The data from TriNet station HEC was obtained through the Southern California Earthquake Data Center (SCEDC); the rest of the data are from the National Strong-Motion Program (NSMP) of the U.S. Geological Survey. The station numbers shown on the map are actually the serial numbers of the recorders; these numbers are used in naming the data files. The official NSMP station numbers are different, but they have not been used, to avoid confusion in relating a station shown on the map with the data file for the time series recorded at that station. Records from all stations shown here were digitally recorded. All but station HEC were digitized using about 4280 counts/cm/sec^2; HEC was digitized at 2140 counts/cm/sec^2. The sensors at all stations are force-balance accelerometers with natural frequency greater than 50 Hz.

record from the whole trace. (As a matter of terminology, we call this the *zeroth-order correction*, and it is understood that all acceleration traces have had this correction performed, even if we state that no baseline correction was done. If no pre-event samples are available, then the mean of the whole record is removed from the trace.) One physical constraint on the ground motion is that the ground velocity be zero, on average, at a sufficiently long time after an earthquake; for this reason, the best way to determine whether there are baseline problems in the recorded acceleration is to look at the velocity obtained by integrating the acceleration. The middle trace in Figure 2 shows the results of doing so. The drift away from zero clearly indicates a baseline problem, and this problem produces a growing displacement (more than 5 m by the end of the record) that is clearly unrealistic. The drift in velocity appears to be a straight line. Fitting a straight line between 37.5 and 67.0 sec yields the line shown in the figure. The slope of the line is consistent with a step change in acceleration of 0.33 cm/sec^2. Note, however, that the line intersects the zero line at 9.5 sec, well before the initial motion (changing the start of the portion being fit from 37.5 to 55.0 sec in 2.5-sec increments resulted in intercept times ranging from 3.6 to 9.9 sec). This indicates that if due to a simple one-time step in acceleration, that step is not associated with the ground shaking. It is more likely that the net baseline offset accumulated from a series of positive and negative offsets over part of the duration of strong shaking. This uncertainty about the details of the baseline offsets is the reason that such offsets are difficult to correct.

Further examples are shown in Figure 3. The top trace is the same acceleration used in the previous figure (the Hector Mine earthquake recorded at HEC), and the second trace is the other horizontal component at HEC. Both components show baseline problems, but the problem is more severe for the east–west component. The bottom two traces are recordings of small earthquakes, with much smaller ground motions than those in the upper two traces. Careful inspection of an enlarged version of the velocity time series for the 21 February 2000 event (Fig. 3b, bottom trace) suggests that the baseline in acceleration had at least four step-like changes, giving rise to four connected line segments in velocity. These examples indicate the difficulty of understanding the true source of the offsets. There are a variety of potential sources, including mechanical (e.g., Shakal and Petersen, 2001) or electrical hysteresis in the sensor, problems with the analog-to-digital converter, and ground tilt and rota-

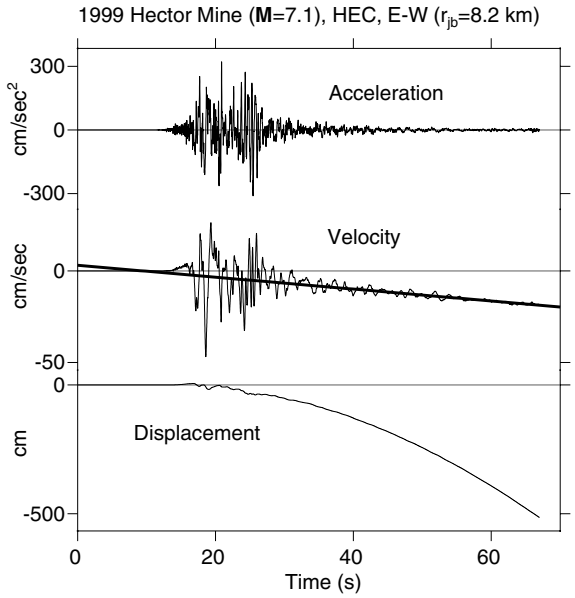

Figure 2. Zeroth-order processing of the east–west component of the accelerogram obtained at station HEC. The top trace is the recorded accelerogram after subtraction of the mean of the pre-event portion of the record; the middle and bottom traces show the velocities and displacements obtained by successive integrations of the top trace. The straight line on the middle trace is the line fit to velocity between 37.5 and 67.0 sec. The unphysical drift in the velocity trace is a tell-tale marker of baseline problems and results in unrealistic displacements. Various baseline corrections for this record are shown in a later figure. r_{jb} is the horizontal distance from the station to the closest point of the surface projection of the rupture surfaces (see Abrahamson and Shedlock, 1997).

tion (e.g., Bradner and Reichle, 1973; Trifunac and Todorovska, 2001), due either to elastic deformation close to large ruptures or to inelastic deformation from slumping or cracking of the earth beneath the recording site. Another source of drifts in velocity and displacement is the accumulation of the random errors in the accelerogram resulting from single and double integration of the random noise; for the velocity trace, this is nothing more than random walk. In the Appendix we derive a formula for the standard deviation of the final displacement, and we show that the resulting standard deviation is much smaller than the observed final displacements obtained by integrating zeroth-order-corrected accelerations. In other words, double integration of random noise is not the cause of the observed drifts in velocity and displacement. The only study we are aware of that tried to pinpoint the source of baseline problems is that of Iwan *et al.* (1985), who found baseline problems for a particular transducer which they attributed to hysteresis occurring primarily when the acceleration exceeded 50 cm/sec^2. This type of hysteresis cannot be the explanation for the offsets occurring in the two recordings of small earthquakes shown at the bottom of Figure 3—the peak accelerations for those recordings are much less than 50 cm/sec^2—nor is it likely to be ground tilt.

Correction Schemes

In view of the difficulty of understanding the exact nature of the baseline shifts for any given record, any correction scheme must necessarily be approximate and empirically based. Because the problems generally manifest themselves at long periods, one simple correction is to apply a low-cut (high-pass) filter to the acceleration records. In many cases that is an acceptable solution. Such a procedure, however, clearly precludes extracting permanent, or as Graizer (1979) calls them, *residual* displacements from the records. It would seem that the high-dynamic-range and broadband instruments currently deployed have the capability to determine the residual displacements close to large earthquakes, and such displacements are useful to seismologists modeling earthquake fault rupture.

In all of the correction schemes discussed here we assume that the recorded trace is directly proportional to acceleration; no correction is made for instrument response. Because the corner frequency of the accelerometer sensor is on the order of 50 times higher than the frequencies controlling ground displacement, the instrument response should be negligible.

Graizer (1979; written comm., 2000) proposed a scheme in which he fit a series of polynomials to the velocity trace, subtracted the derivative of each polynomial from the acceleration, and then looked at the resulting displacement trace. He made a subjective judgment about which polynomial gave the best results.

Boore (2001) discusses a slight generalization of a scheme published by Iwan *et al.* (1985). The Iwan *et al.* scheme is based on the notion that the baseline may have complicated and perhaps random shifts during the interval of strong shaking, but that these shifts can be represented by an average baseline correction over this interval. This scheme is illustrated in Figure 4. With the constraint that the average velocity at the end of the record be zero, the scheme involves fitting a straight line to velocity for some portion after the strong shaking has ceased and then connecting this straight line with another line starting from zero velocity at time t_1 near the beginning of the motion and joining the fitted line at the later time t_2. Figure 4 shows the lines for three values of t_2 for an actual application. As shown in Figure 5, the correction of the acceleration is given by subtracting the slopes of the velocity lines. If the latter part of the uncorrected velocity time series is well represented by a straight line, then this correction procedure guarantees that the latter part of the displacement time series derived from the corrected acceleration trace will be flat. It will then look realistic (a portion of strong shaking followed by a constant residual level), but the realistic appearance of the time series does not mean that it is correct. The residual level can depend strongly on the processing parameters (for example, Figure

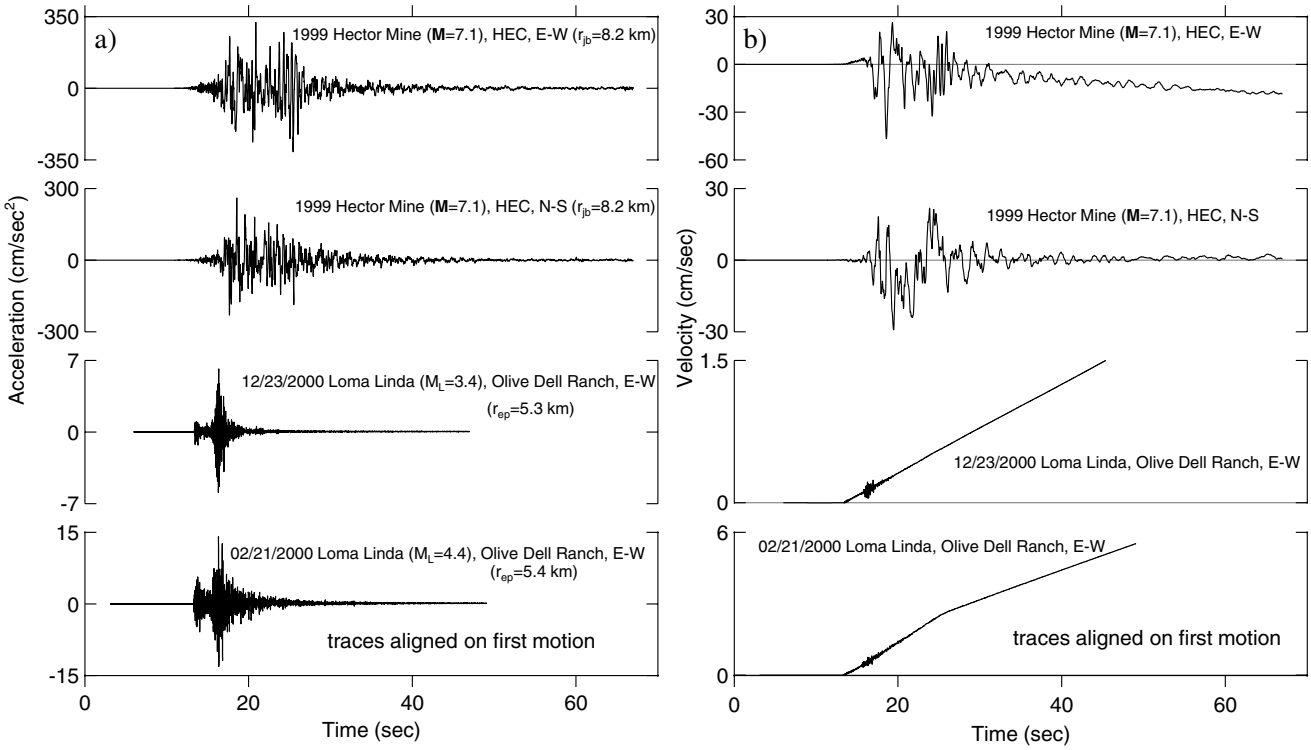

Figure 3. (a) horizontal-component acceleration traces, after zeroth-order correction, for one large and two small earthquakes; (b) velocity traces derived from integration of the accelerations shown in (a). The drifts in the velocities indicate baseline problems. Note that the baseline problem is different for the two horizontal components of the HEC recording and that the problems can occur for very small as well as large ground accelerations. r_{ep} is the epicentral distance; r_{jb} is as defined in the caption to Fig. 2.

6 shows that the residual displacement can be sensitive to parameter t_2).

From our experience with records from a number of earthquakes, the baseline corrections might be more complicated than given by the simple two-level correction. For example, fitting four lines to the bottommost velocity time series shown in Figure 3b yields a reasonable displacement time series (we demonstrate this at the end of the article). When many records are suddenly made available, however, such as following a large earthquake, it is not feasible to tailor the baseline correction to each recording. This happened to us after the 1999 Hector Mine earthquake, and we adopted the following simple scheme for processing those records; variations of this scheme have been used in processing the records from subsequent earthquakes. The scheme involves fitting a quadratic to the velocity and then filtering, as outlined below:

1. Compute mean of the pre-event portion of the record (stopping a second or so short of the estimated first arrival) and subtract that mean from the whole record (the zeroth-order correction).
2. Integrate to velocity.
3. Fit a quadratic to velocity, starting at the time of the first arrival and constrained to be 0.0 at the start time.
4. Remove the derivative of the quadratic from the zeroth-order-corrected acceleration.
5. Apply a causal, low-cut Butterworth filter with a subjectively chosen corner frequency.
6. Integrate to velocity and displacement.

An important advantage of digital records is that for most recordings pre-event samples are available, and thus the initial conditions for velocity and displacement are approximately known. In this case it makes sense to use a constrained quadratic. Data obtained from triggered analog instruments or from digital instruments that triggered late enough into the record do not have this advantage, and the choice of initial velocity is a vexing problem not discussed in detail here.

Some care must be used in specifying the portion of the velocity record for which the quadratic is to be fit, particularly if the record is very long. For a long record, a quadratic may be a poor approximation of the drift in the velocity trace over the whole duration of the motion, and forcing a fit over the whole duration will likely result in unacceptable distortions in the important portion of record.

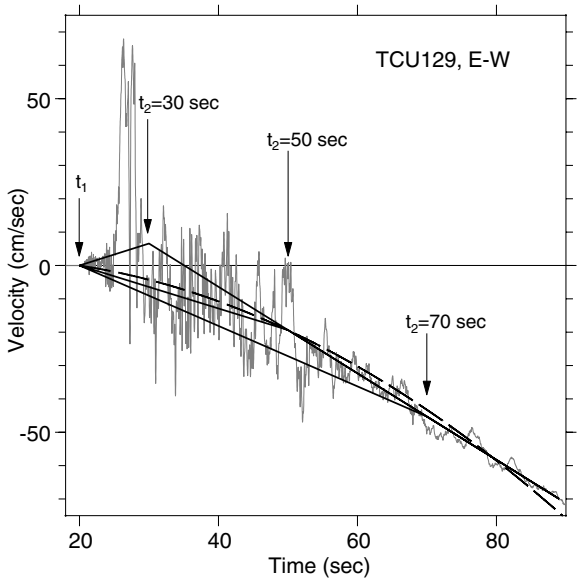

Figure 4. Shaded line: velocity from integration of the east–west component of acceleration recorded at TCU129, 1.9 km from the surface trace of the fault, from the 1999 Chi-Chi, Taiwan, earthquake, after removal of the pre-event mean from the whole record. A least-squares line is fit to the velocity from 65 sec to the end of the record. Various baseline corrections are obtained by connecting the assumed time of zero velocity t_1 to the fitted velocity line at time t_2. Three values of t_2 are shown: 30, 50, and 70 sec. The dashed line is the quadratic fit to the velocities, with the constraint that it is 0.0 at $t = 20$ sec. (Modified from Boore, 2001.) The acceleration time series are obtained from a force-balance transducer with natural frequency exceeding 50 Hz, digitized using 16.7 counts/cm/sec^2 (16,384 counts/g).

In some cases the baseline correction alone yields reasonable-looking displacements (a subjective judgment, to be sure, but one that we see no way of avoiding), but in other cases undesirable long-period oscillations occur. We find that the displacement traces for the USGS digitally recorded data from the Hector Mine earthquake were improved by applying a filter with 0.02-Hz corner frequency. This is a frequency low enough that essentially no information of importance to the engineer is lost. (We could use such a low frequency because the earthquake was large enough to be rich in long periods and because the digital instruments have a large dynamic range.) We use a causal filter because it avoided peculiar-looking precursory transients that exist if an acausal filter is used. As shown later, the price paid is that the detailed shape of the waveforms can be quite sensitive to the filter corner frequency. We also use a fourth-order Butterworth filter, with a response decaying as f^4 at low frequencies. The response of a lower-order filter might not decay rapidly enough to overcome the increase of noise with decreasing frequency (which for a step in acceleration goes as $1/f^3$ for displacement); a higher-order filter might produce ringing. To our knowledge, the filter used for the USGS digital data from the Hector Mine earthquake has a much lower corner frequency used in any processed strong-motion data previously made available to the public for this or any other earthquakes. In our procedure, the acceleration, velocity, and displacement time series are each filtered only once, unlike some other processing schemes (e.g., Lee and Trifunac, 1984; Huang *et al.*, 1989; Chiu, 1997).

Figure 4 shows the quadratic fit to the velocity trace in that figure, and Figure 5 shows the resulting correction to the acceleration trace. The displacement resulting from both the two-line and the quadratic schemes for the record in Figure 3 are shown in Figure 6. Also shown in Figure 6 are the displacements resulting from removing only the mean (the zeroth-order correction) and from only low-cut filtering the record, as well as the permanent displacement from a GPS station 2.3 km from the seismic station. Obviously, the range of residual displacements is enormous, and lacking GPS or some other independent measurement of the residual displacement at a site, it is not possible to choose the optimal correction scheme (and what is correct for one station most likely is not correct for other stations). Fortunately, as Boore (2001) shows, the response spectra for the accelerations corrected as in Figure 6 are almost identical for oscillator periods less than about 20 sec. There are few engineering structures affected by such long periods, and therefore the choice of which correction scheme to use is largely irrelevant for most engineering purposes, at least for most recordings of large earthquakes recorded on high-quality instruments. (Boore [2001] shows an exception for a record whose spectrum is unusually enriched in energy around 1-sec period, either because of a local site response or because of an instrument malfunction.)

Modifications of the constrained quadratic scheme are almost endless. For example, the quadratic can be fit to a portion of the record after the strong shaking has ceased. Another obvious modification is to use higher-order polynomials; this is essentially Graizer's method (Graizer, 1979), with the difference that the polynomial is constrained to be zero at the first-arrival time. As a final example, an unconstrained, rather than a constrained, quadratic might be used. For a few digital recordings of the 1999 Hector Mine earthquake at USGS stations, the instruments triggered late enough that no pre-event samples were available. For the processing of these USGS data for public distribution we sometimes used an unconstrained fit because it gave better-looking motions near the beginning of the record; in such cases, the initial velocity is determined by the quadratic fit and is not zero. If an unconstrained quadratic is used for a record with pre-event samples, it requires adding an impulse to the acceleration trace at the time t_1 for which the corrections are first applied (usually the first-arrival time). In lieu of this, we use the negative of the zero-time intercept of the unconstrained quadratic as an initial velocity in the acceleration to obtain velocity and displacement. Furthermore, to capture the effect of the initial velocity, the filtering must be done on the acceleration, velocity, and displacement traces

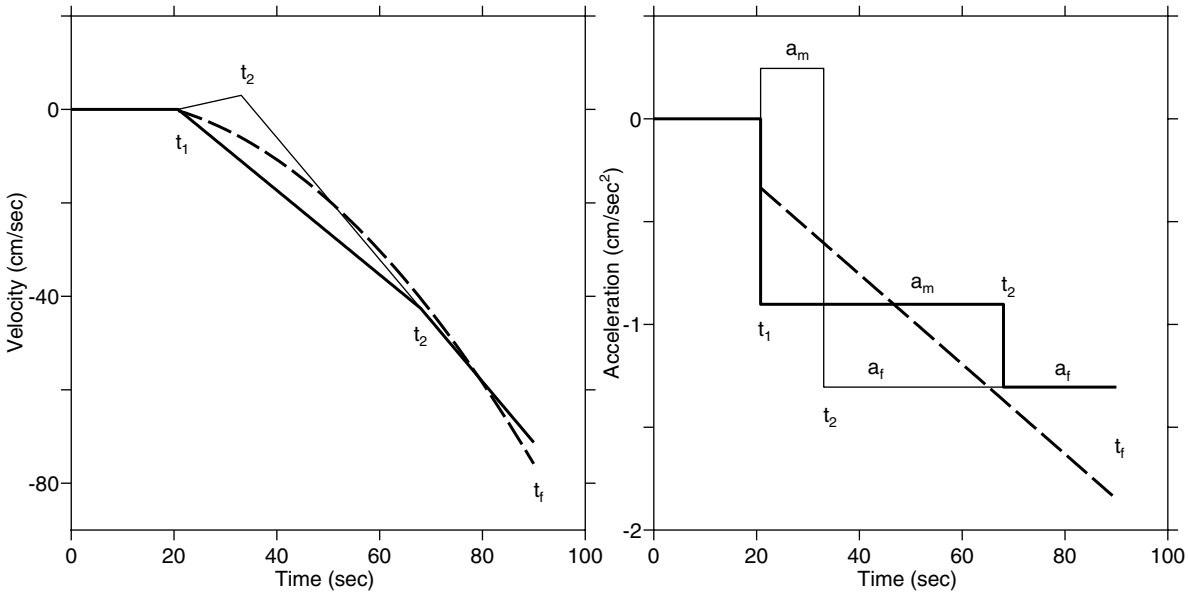

Figure 5. Basis of Iwan *et al.* (1985) baseline-correction scheme, as discussed in Boore (2001). The light and heavy lines are for two choices of t_2. The dashed line in the left plot is the quadratic fit to the velocity; the derivative of that quadratic is the baseline correction applied to the acceleration trace—this is shown by the dashed line in the right plot. (Modified from Boore, 2001.)

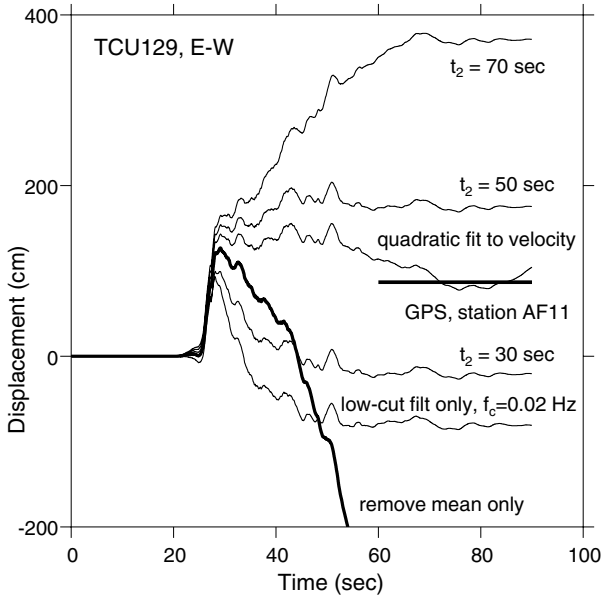

Figure 6. Displacements obtained by double integration of the east–west component of acceleration recorded at TCU129 from the 1999 Chi-Chi, Tawian, earthquake and modified using a variety of baseline corrections. The GPS level was obtained at a station 2.3 km from TCU129, above the footwall of the fault (as is TCU129). (Modified from Boore, 2001.)

individually (where the velocity and displacement are obtained from the unfiltered acceleration). Except for this special case, experiments show that the order of filtering and integration is not important, as expected for operations on linear systems.

Examples from the 1999 Hector Mine Earthquake

We now show a number of examples of the results of processing records from the **M** 7.1 1999 Hector Mine earthquake, using data primarily from the U.S. Geological Survey (available from *http://nsmp.wr.usgs.gov*). The first example shows the result of baseline correction with no filtering, and the rest of the examples show the results of the quadratic-plus-filtering scheme discussed above.

Attempting to Recover Permanent Displacements: Station HEC

Residual displacements obviously are impossible to obtain if low-cut filtering is used. In most cases, this is of no consequence, but when a high-quality recording is obtained close to an earthquake, an attempt should be made to recover the residual displacement. Such a case is the HEC recording of the 1999 Hector Mine earthquake (see Fig. 1). The station is operated by the Southern California Seismic Network, part of TriNet (Graizer *et al.*, 2002). We show in Figures 7 and 8 the consequences of the constrained quadratic and the two-line correction schemes for the two horizontal components

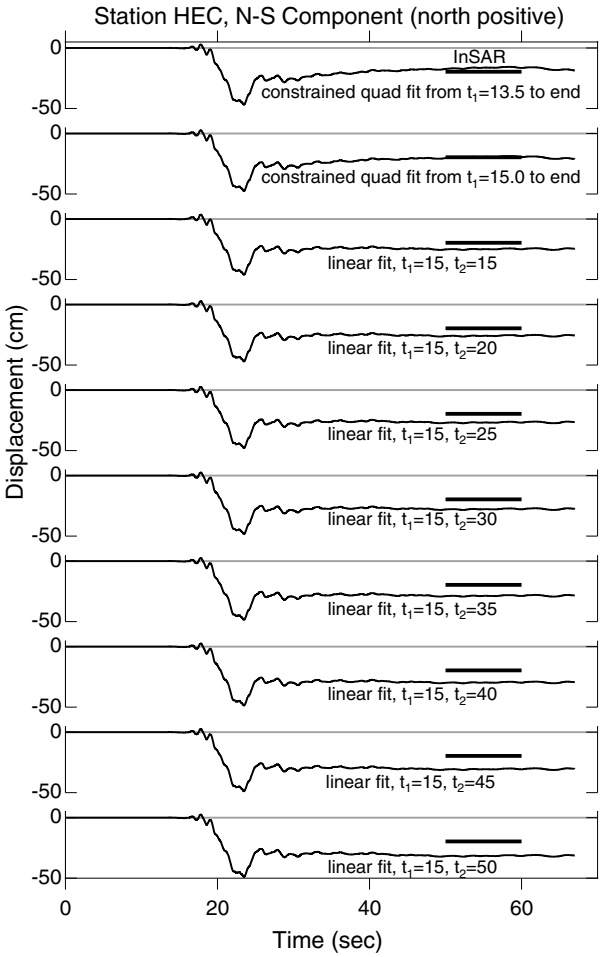

Figure 7. Unfiltered displacements at station HEC derived from the north–south component of acceleration corrected according to a constrained quadratic fit to the velocity for the indicated times and to the two-line correction with a number of choices of t_2, with the linear fit to velocity from 37.5 to 67 sec for all cases. The short, heavy bars plotted along with each trace show the estimate of the ground displacement obtained from analysis of interferometric synthetic aperture radar (InSAR) data (courtesy of Y. Fialko, written comm., 2001). The InSAR value is the average of 9 pixels centered on HEC.

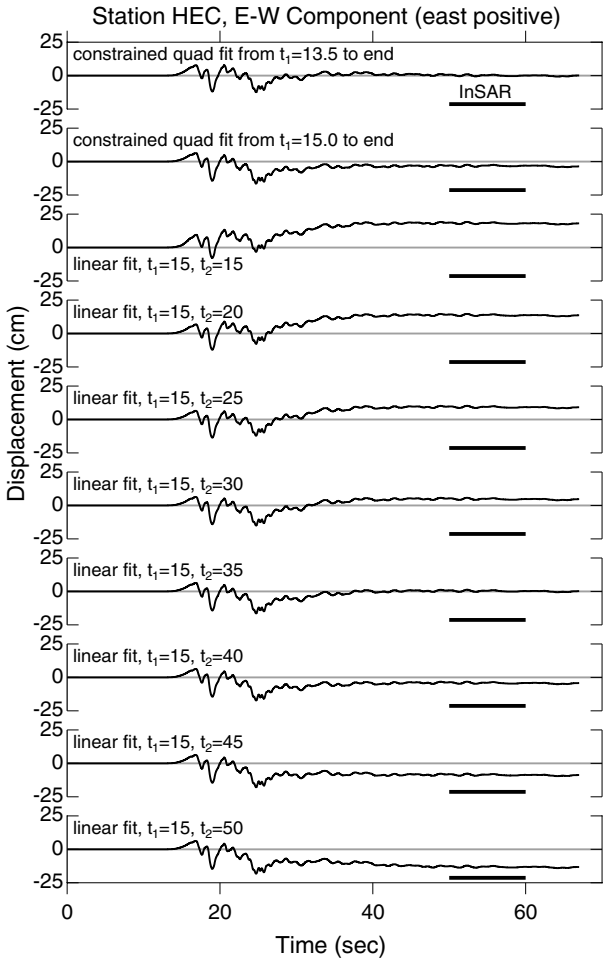

Figure 8. Unfiltered displacements at station HEC derived from the east–west component of acceleration corrected according to a constrained quadratic fit to the velocity for the indicated times and to the two-line correction with a number of choices of t_2, with the linear fit to velocity from 37.5 to 67 sec for all cases. The short, heavy bars plotted along with each trace is the estimate of the ground displacement obtained from analysis of InSAR data (courtesy of Y. Fialko, written comm., 2001). The InSAR value is the average of 9 pixels centered on HEC.

obtained at this site. Also shown in the figures are the estimates of the displacements obtained from analysis of interferometric synthetic aperture radar (InSAR) data. These displacements are from Y. Fialko (written comm., 2001; see also Fialko and Simons, 2001), who considers them to be coseismic; he estimates that the error is less than 5 cm, with the east–west displacement being more accurate than the north–south displacement. Because they level out to a more-or-less constant residual value, all of the baseline-corrected displacements look correct, but that is not an adequate reason to accept the results of a particular correction. The north–south component is more stable, and the residual displacements are close to the InSAR-derived value; such is not the case for the east–west component, however. It may be recalled from Figure 3b that the east–west component had the more obvious drift in the velocity trace. If the InSAR-derived displacement is correct, then none of the baseline-correction schemes is a good approximation of the actual baseline distortions on the east–west component.

As we mentioned earlier, a consequence of the baseline correction scheme used to produce the displacements in Figure 8 is a flat residual displacement, even if long-period noise is present. Experiments that we have done with low-cut filtering of a step function suggest that, to define an apparently level time series of duration T, the period content

of the ground motion must extend to at least 20*T* (for example, *T* for the HEC displacements is about 40 sec, so periods of almost 1000 sec are needed to define the step). Any noise at these long periods will map into the level of the residual displacements. One possible source of such noise is the rotation and torsion of the ground associated with elastic wave propagation, as pointed out by Trifunac and Todorovska (2001). These ground motions will cause baseline distortions in recorded accelerations, even in the absence of other sources of distortions, and Trifunac and Todorovska (2001) conclude that "it is not possible to compute accurately and reliably permanent displacements of the ground . . . without simultaneously recording rotations during strong motion." Figure 7 in Trifunac and Todorovska (2001), however, shows that the effects of rotation and torsion should be negligible for frequencies greater than 0.001 Hz (1000 sec) at a distance of 10 km from a magnitude 7 earthquake (essentially the situation for the HEC recording). This is barely at the period limit mentioned for the definition of an apparently flat residual displacement of 40 sec duration. In addition, we note that the rotation- and torsion-induced distortions should be very small after the strong shaking has ceased; for this reason, the accumulated effect would be a finite-duration offset in the acceleration, which would integrate to a postshaking flat velocity trace and not to the ramp seen for the HEC data (Fig. 3b). We conclude that, although they are undoubtedly present, distortions due to rotations and torsions are not as important as other causes of baseline offsets for the HEC recording.

Comparison of Waveforms

We now turn to examples for stations farther from the fault. In these cases we made no effort to recover residual displacements, and we filtered all records using a corner frequency of 0.02 Hz. One way of checking the results is to compare the displacements at stations located close to one another (Hanks, 1975). We do this for three sets of stations, at generally increasing distance from the fault.

The first comparison is for stations 514 and 588, separated by 6.9 km (see Fig. 1 for locations of these and other stations discussed in this section). Figure 9 shows the results. The north–south component shows the best comparison, and the comparison provides some confidence in the choice of processing used for the records. Both horizontal components are similar in shape, indicating that the ground displacement has a strong linear polarization in the northwest–southeast direction, and thus they are largely SH waves. The vertical displacements at the two stations also compare well; they are much smaller and have a much different waveform than the horizontal displacements.

The next comparison is for stations 513, 521, and 530, which are arranged more or less along a line of constant azimuth from the source. While not particularly close together (22.5 km for the 513–521 pair and 15.3 km for the 521–530 pair), the stations are underlain by roughly similar geologic materials. The stations are along the northern base

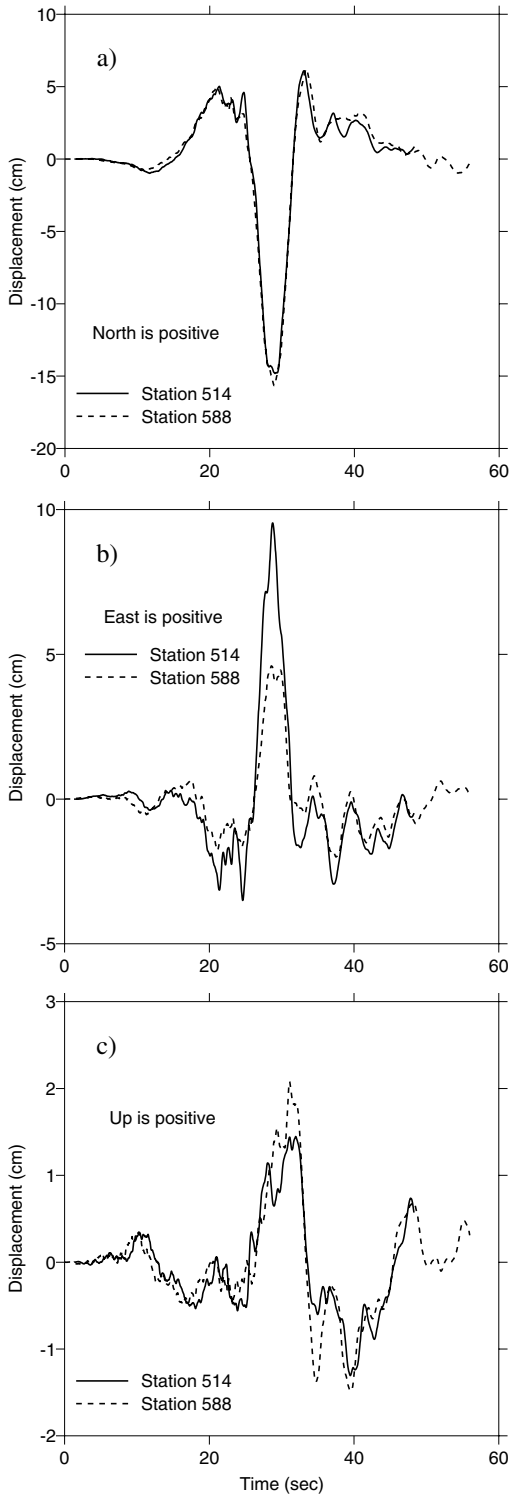

Figure 9. Comparison of displacements derived using a constrained quadratic fit to the whole velocity record, and filtered using a causal fourth-order, low-cut Butterworth filter with a 0.02-Hz corner frequency. This is the same processing used for the data available on the USGS NSMP Web site (*http://nsmp.wr.usgs.gov/*). The traces are aligned using time shifts derived by aligning the large pulse to the south on the north–south component. The two stations are separated by 6.9 km. The north–south, east–west, and vertical displacements are shown in parts (a), (b), and (c), respectively. Note difference in amplitude scales, particularly horizontal vs. vertical.

of the San Gabriel Mountains at the southwestern edge of the Mojave Desert. The comparisons of displacements are shown in Figure 10. Uncorrected displacements for the north–south components are shown in Figure 10a, and comparisons of displacements derived from the corrected accelerations are given in Figure 10b–d for the three components of motion. The displacements at stations 513 and 521 suggest that the recorded motions are remarkably free of baseline-offset problems; on the other hand, the displacement trace for station 530 shows a clear drift. This drift looks linear, which could be produced by a single spike in the acceleration. The slope of the linear trend in displacement is about 0.25 cm/sec. Given the time spacing of 0.005 sec, a step of 0.25 cm/sec would be produced by a single acceleration spike of $0.25/0.005 = 50$ cm/sec^2. This is comparable to the peak acceleration for this record (51.9 cm/sec^2). Plots of the acceleration time series (not shown here) using a series of narrow time windows, however, indicate no individual spikes. Thus, the drift must be produced by some other feature.

As in the previous comparison (stations 514 and 588), the displacements for each component are reassuringly similar. What is remarkable, however, are the differences in waveforms between components. Both the east–west and the vertical components have an early phase that has an apparent velocity higher than the phase on which the traces are aligned. As these components are more favorably oriented to be affected by *P* energy than is the north–south compo-

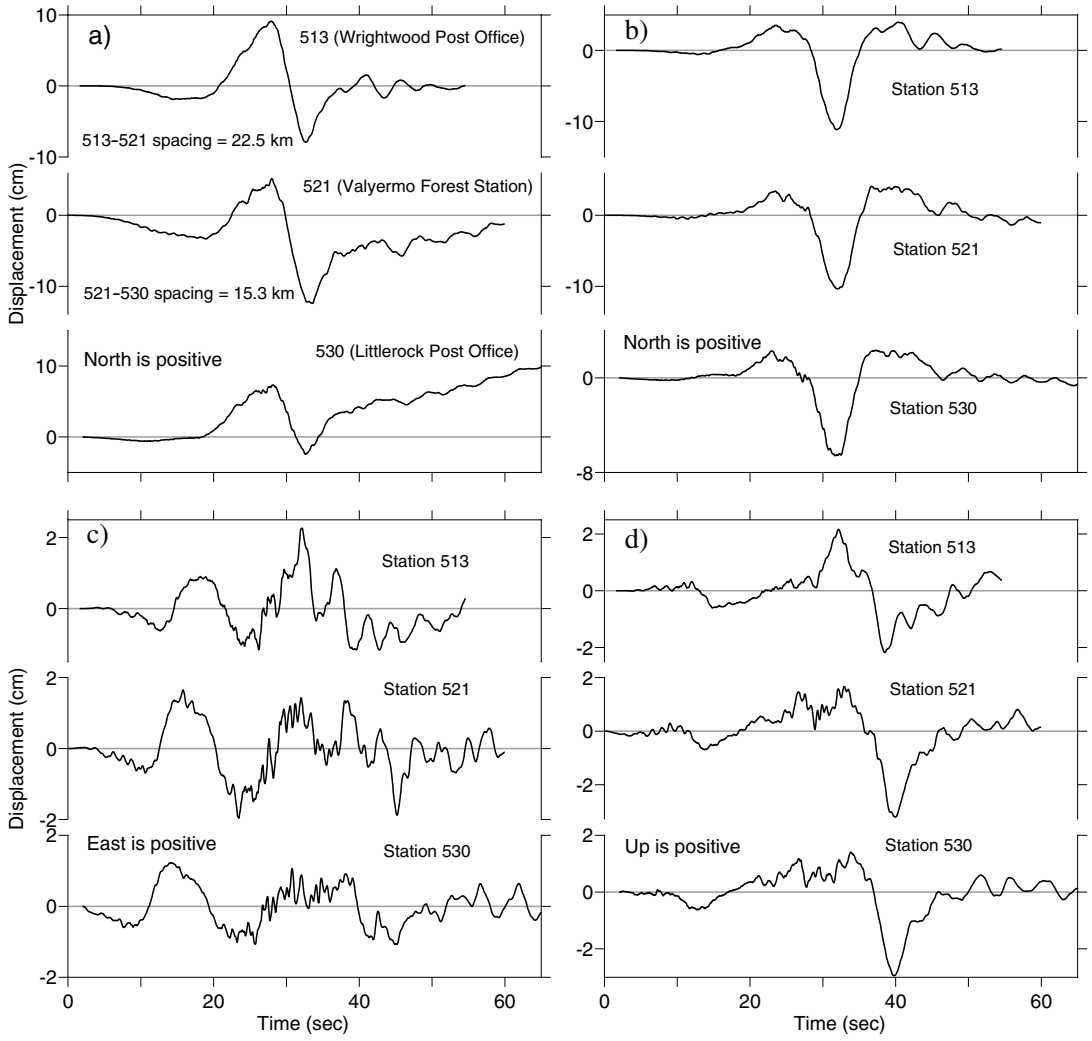

Figure 10. Comparison of displacements from three stations separated by larger distances (22.5 and 15.3 km) than that in the previous figure. (a) North–south displacements from accelerograms with zeroth-order processing; (b), (c), and (d) displacements for all components, from accelerograms processed using the constrained quadratic fit to velocity and causal low-cut filtering with a 0.02-Hz corner frequency. Note the large difference in peak amplitudes between the three components, with the north–south component being much larger. The traces are aligned using time shifts derived by aligning the large pulse to the south on the filtered north–south component.

nent (which is probably dominated by the SH radiation from the source), it is likely that this earlier phase contains a significant amount of *P* energy. What is also striking is the dissimilarity of the east–west and vertical components at these stations and those at stations 514 and 588 (although the north–south components are similar). It may be that the line of stations crosses radiation pattern nodes, a subject beyond the scope of this article. We suggest that these data will be of interest to those modeling the earthquake source.

One caution for those modeling the U.S. Geological Survey's processed data from the Hector Mine earthquake (data from *http://nsmp.wr.usgs.gov*): the causal filter produces significant phase distortions that can make the shape of the displacement waveforms quite sensitive to the corner frequency of the filter. This is illustrated in Figure 11a. As shown in Figure 11b, however, the velocity waveforms are much less sensitive to the baseline corrections and filtering. Most modeling studies invert the velocity waveforms and therefore will not be strongly affected by the filter distortions. Nevertheless, it would be prudent for modelers to apply the same filter used in the data to their synthetic motions.

In spite of the large differences in the displacement waveforms shown in Figure 11a, the response spectra derived from the accelerations from which the displacements in Figure 11a were derived are similar for periods less than about 20 sec (Fig. 12). The differences in the 2- to 6-sec range are related to a hole in the Fourier amplitude spectrum for this range of periods. An oscillator of a given period responds to other ground-motion periods if the ground motion is lacking energy at the oscillator period. Because both the oscillator frequency response and the ground-motion spectrum have complicated shapes, this can make it difficult to predict the relative behavior for a series of ground motions.

The final example of a comparison of waveforms is for stations 596 and 1099. These stations are separated by only 1.6 km and are sited on similar geologic conditions. The comparison is only for the north–south component. The zeroth-order-corrected acceleration trace and the velocity and displacement traces derived from this acceleration trace are shown in Figure 13. As with the previous comparison, the displacement for one station (1099) shows a drift, while

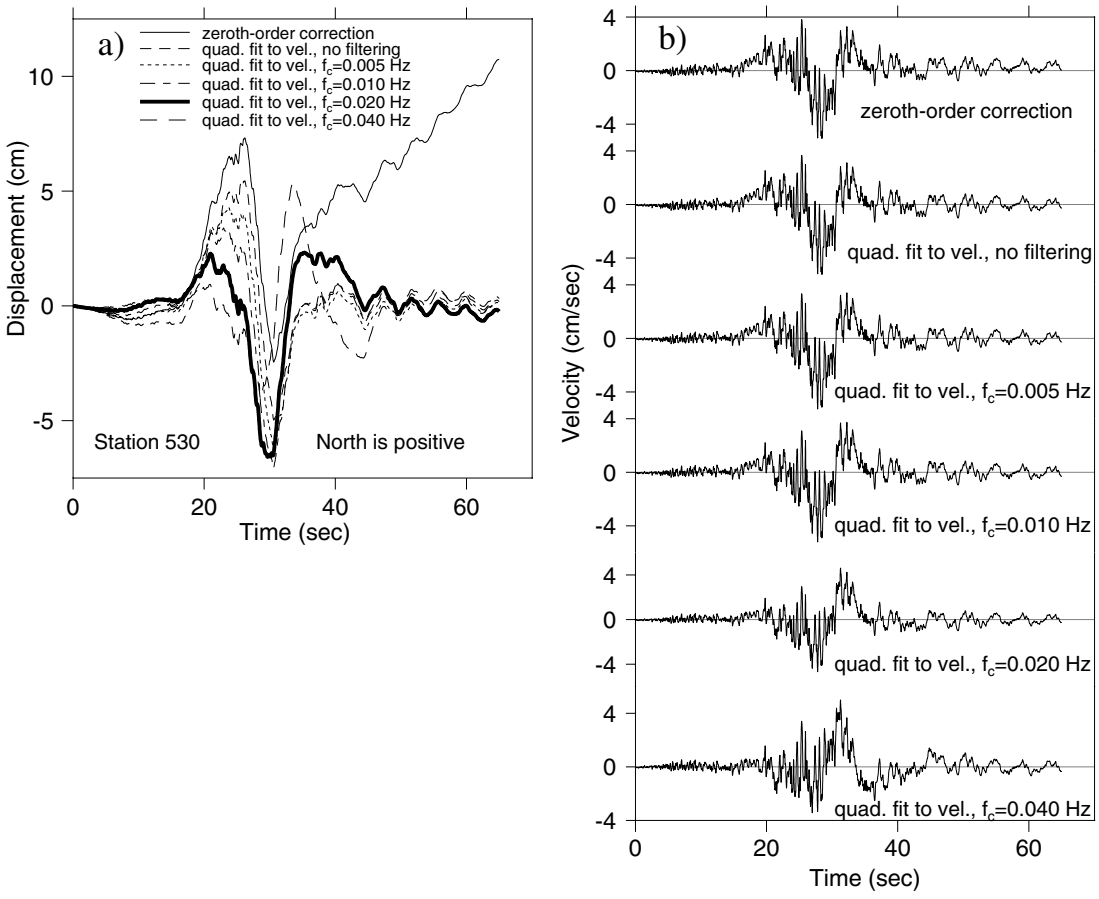

Figure 11. (a) Displacements and (b) velocities for one of the stations used in the previous figure, showing the effect on the waveforms and spectra of different filter corner frequencies (f_c). The heavy line in panel (a) shows the data available from the NSMP Web site. The velocities are much less sensitive to the baseline correction and low-cut filtering than are the displacements.

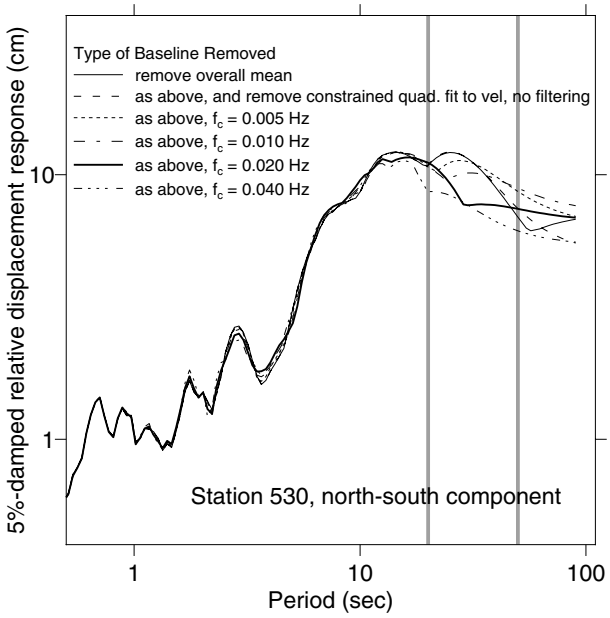

Figure 12. Five-percent-damped relative-displacement response spectra from accelerations corrected as indicated in Fig. 11. The heavy line corresponds to the data available from the NSMP Web site. For reference, the two gray lines are drawn for periods of 20 and 50 sec.

that from the other station (596) is well behaved. The velocities and displacements for the corrected accelerations are compared directly in Figure 14. The comparison is very good, again attesting to the effectiveness of the processing scheme and to the high quality of the data.

The previous figures show a pronounced pulse in displacement on all of the stations. This pulse is a pervasive feature of the earthquake, as shown in Figure 15. That figure contains plots of the displacements rotated into a direction transverse to the path between the station and the epicenter. The radial displacements (Fig. 16) are neither as uniform in shape nor as large as the transverse displacements. Apparently most of the ground displacement is carried by SH waves. The SH pulse leads to pseudovelocity response spectra that do not start to decay toward the long-period displacement-controlled asymptote until periods of about 10 sec are reached (Fig. 17). This period is significantly larger than the 4-sec transition period included in some recent building codes (e.g., BSSC, 1998; see also Bommer and Elnashai, 1999). Until the recent digitally recorded earthquakes, strong-motion data have not had sufficient signal–noise amplitudes to allow trustworthy estimates of ground motion beyond about 5 sec. As a result, ground-motion prediction equations have been limited to response spectra less than about 5 sec. The predictions for the Abrahamson and Silva (1997) equations are given in Figure 17; their predictions are consistent with the Hector Mine earthquake data.

A Record of Structural Response

The last example of data from the 1999 Hector Mine earthquake is a record obtained on the 12th floor of a 12-story building. The acceleration is shown at the top of Figure 18a. Note that the decision to stop recording was based on the output of a sensor in the basement of the building. Obviously, the algorithm for determining when to cease recording was not appropriate, for much of the response of the top floor of the building was lost. This record illustrates why baselines should be determined by fitting curves to velocity rather than acceleration. The second and third traces from the top show the velocity traces obtained by removing the mean and the best-fitting straight line to the acceleration,

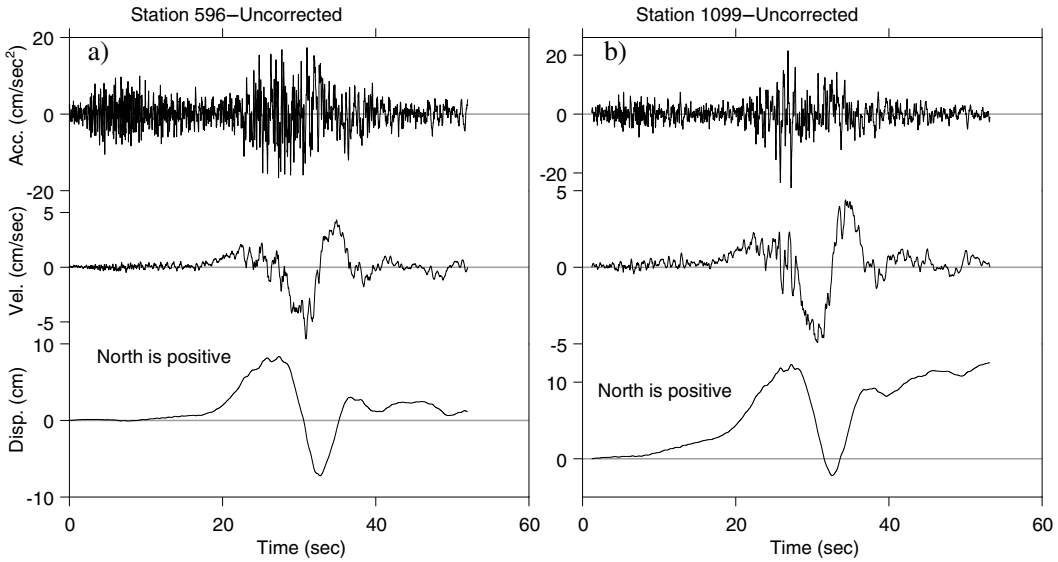

Figure 13. Zeroth-order-corrected accelerations and associated velocities and displacements at two closely spaced (1.6 km) stations: (a) station 596; (b) station 1099.

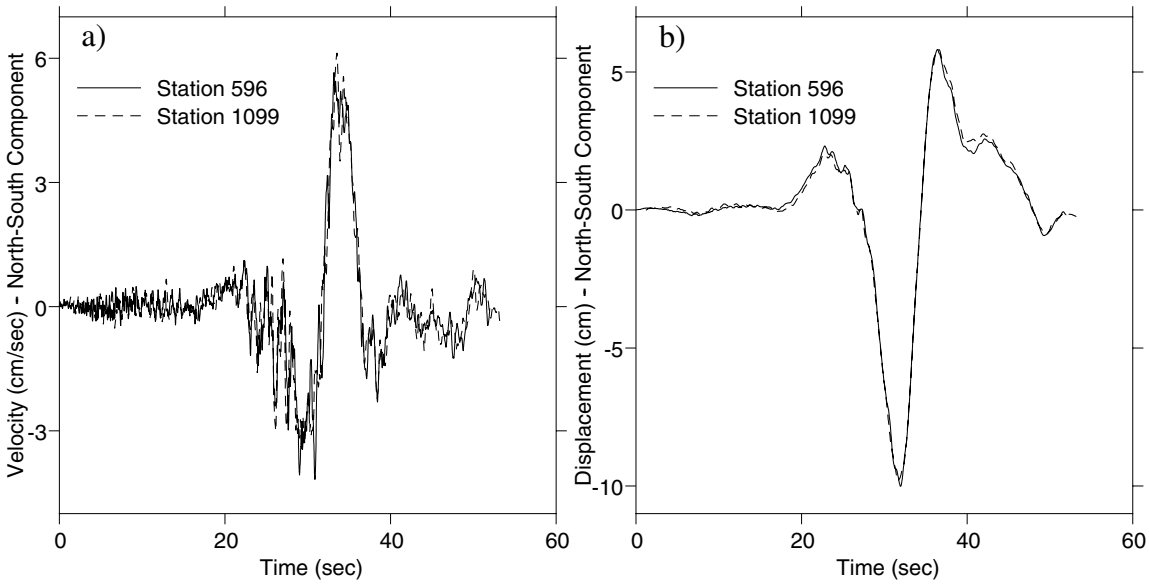

Figure 14. Comparison of (a) velocities and (b) displacements for the two closely spaced (1.6 km) stations of Fig. 13. The recorded accelerations from which the velocities and displacements are derived were processed using a constrained quadratic fit to velocity, followed by causal filtering with a corner frequency of 0.02 Hz. The traces are aligned using time shifts derived by visually aligning the large pulse to the south on the displacement trace.

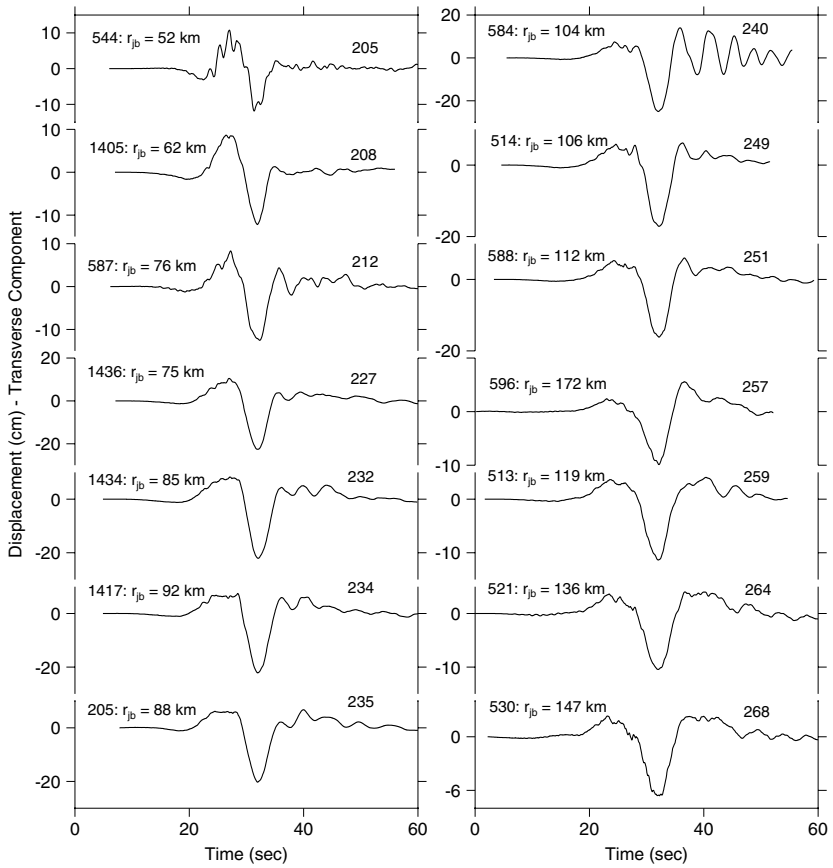

Figure 15. Transverse displacements, relative to the epicenter, arranged by azimuth (see Fig. 1). The station number is given to the left of the distance r_{jb}, and the epicenter-to-station azimuth, in degrees clockwise from north, is given above and to the right of each trace. The distance r_{jb} is as defined in the caption to Fig. 2. Transverse is positive to the left looking toward the source from the station. The transverse displacements are obtained by rotating the displacements derived from the corrected, unrotated accelerations.

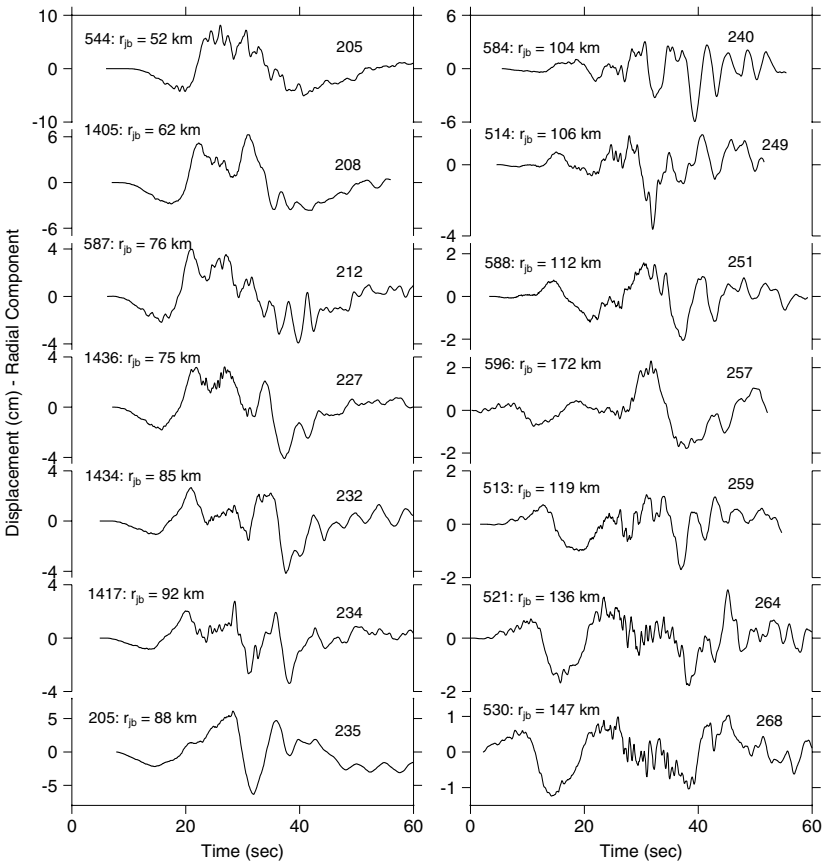

Figure 16. Radial displacements, relative to the epicenter, arranged by azimuth (see Fig. 1). The station number is given to the left of the distance r_{jb}, and the epicenter-to-station azimuth, in degrees clockwise from north, is given above and to the right of each trace. The distance r_{jb} is as defined in the caption to Fig. 2. Radial is positive in the direction of a line from the epicenter to the station. The radial displacements are obtained by rotating the displacements derived from the corrected, unrotated accelerations.

respectively. By doing so, it is guaranteed that the overall mean of acceleration equals 0.0, and therefore velocity is equal to 0.0 at the end of the record. This obviously is not what is desired in this case. The bottom three traces show the velocities derived from accelerations corrected by subtracting from the zeroth-order-corrected acceleration trace the derivative of first- and second-order polynomials fit to the uncorrected velocity trace. These corrected velocity traces are very reasonable, oscillating about 0.0 at the end of the record. The displacements derived from the corrected accelerations are compared directly in Figure 18b, and the response spectra are compared in Figure 19. Again, we find that large differences in the ground displacements due to various processing schemes have little effect on the ground motions at periods of engineering interest.

Example from the 21 February/2000 Loma Linda Earthquake

We now discuss processing of the bottom trace shown earlier in Figure 3, for which the velocity trace suggests a series of small step changes in acceleration. Our motivation is to see how well the generic quadratic-fit, filtering approach, or just filtering alone, will work on a record such as this. The comparisons of the derived velocities and displacements are shown in Figures 20a and 20b. Filtering alone, or in combination with removal of a constrained quadratic fit to velocity, gives unrealistic-looking waveforms. This is not surprising in view of the character of the uncorrected velocity, which indicates that a series of four steps occurred in the acceleration. Choosing the times of these steps from visual inspection of the top trace in Figure 20a, we made corrections based on a sequential series of constrained linear lines fit to the velocity traces (this correction could be determined in one step by finding the coefficients of a series of hinged straight line segments). The bottom two traces in Figure 20 show the results of this correction with and without filtering. Subjectively, the bottom trace looks the best, although we have no way of knowing if the oscillations in the displacement trace are real or not. The period of the late oscillation in the bottom trace is about 10 sec, whereas the filter period is 14.3 sec; thus, the oscillation probably is not a filter transient. Note the low amplitude of the peak displacement: about 0.01 cm.

It is interesting to note that, although the velocity waveforms are somewhat different, the peak motions are rather similar (except for the uncorrected velocity shown as the top trace of Fig. 20a). This is good news, for it means that rou-

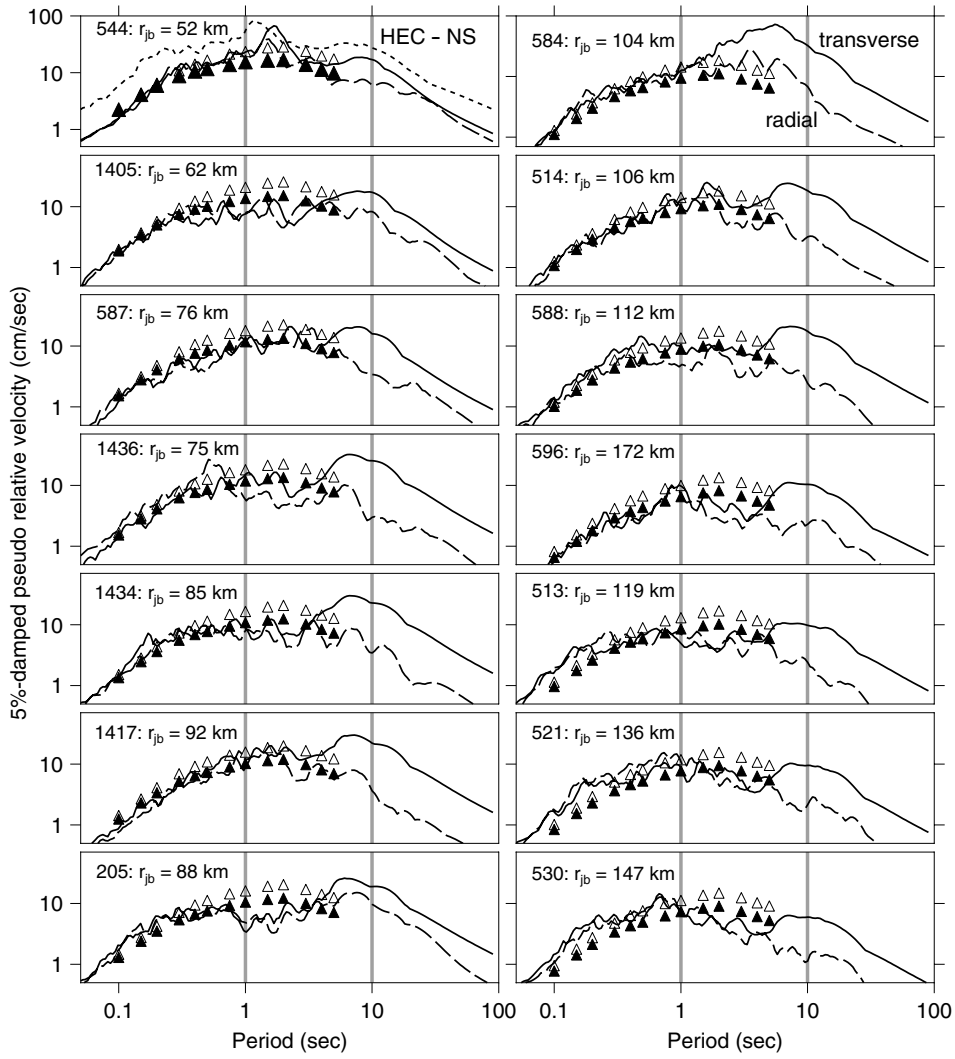

Figure 17. Five-percent-damped pseudo-relative-velocity response spectra computed from corrected accelerograms rotated into transverse (solid line) and radial (dashed line) components. The station number is given to the left of the distance r_{jb}, and the epicenter-to-station azimuth, in degrees clockwise from north, is given above and to the right of each trace. The distance r_{jb} is as defined in the caption to Fig. 2. Also shown is the response spectrum from the north–south recording at station HEC (short-dashed line in upper left graph). All response spectra are from accelerations low-cut filtered at 0.02 Hz. In addition, predictions from the empirical equations of Abrahamson and Silva (1997) are shown, assuming both rock (solid triangle) and soil (open triangle) site conditions. No predictions are available for periods greater than 5 sec. The Abrahamson and Silva (1997) predictions are for the median of the horizontal spectral amplitudes at a given period, not the larger of the two horizontal amplitudes. We use velocity response in order to show the comparison over a wide period range with a minimum range of the ordinate.

tine processing can yield peak velocity values that can be used for the construction of ShakeMaps (Wald *et al.*, 1999); corrections tailored to the data may not be needed. This cannot be said for the peak displacement, however. As shown in Figure 20, the waveforms and the peak displacements are quite different (the traces are plotted with individual scaling). The response spectra for the corrected accelerations are shown in Figure 21. As judged from Figures 20 and 21, the tailored correction based on fitting a series of line segments goes a long way toward removing the baseline problem, even without filtering. Note that, even for such a small earthquake, the digital recording seems to give good information for periods as long as about 10 sec and for displacements as small as 0.01 cm.

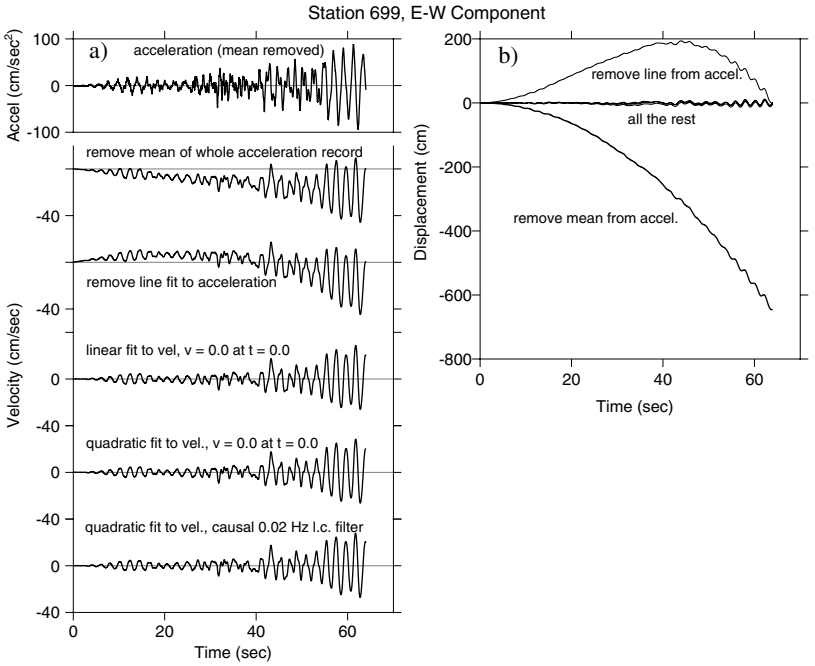

Figure 18. (a) Velocities and (b) displacements obtained from various processing schemes applied to the acceleration shown at the top of panel (a); all traces below the top trace in (a) are velocities. The acceleration time series was obtained from the top floor of a 12-story building (Station 699 in Fig. 1); the time to stop recording was controlled by the accelerations from a sensor at the base of the building, and therefore the recording was terminated prematurely. "l.c." stands for "low-cut."

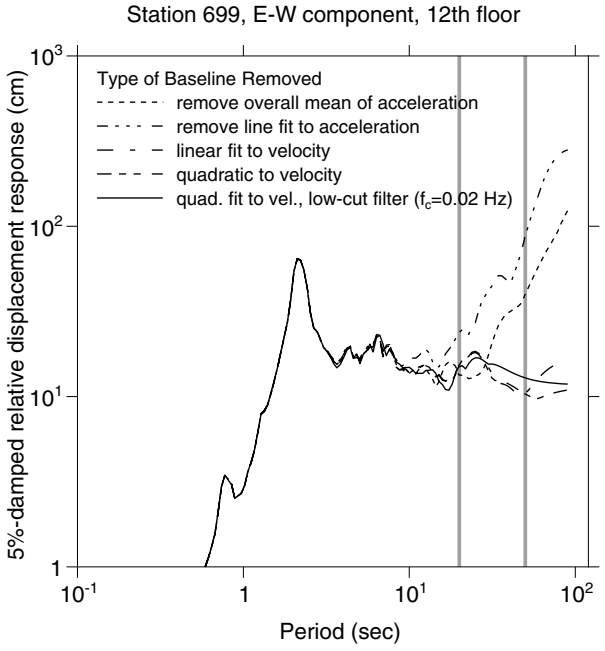

Figure 19. Five-percent-damped relative-displacement response spectra from the accelerations processed as in Fig. 18. The acceleration corresponding to the solid line was obtained using a causal fourth-order Butterworth low-cut filter with corner frequency of 0.02 Hz. For reference, the two gray lines are drawn for periods of 20 and 50 sec.

Discussion and Conclusions

Contrary to what might reasonably be assumed, digitally recorded data usually need corrections for offsets in the acceleration baseline. Unfortunately, there is no universal cure for baseline afflictions. A correction scheme can be tailored by studying the character of the velocity obtained by integration of zeroth-order-corrected acceleration, and then seeing if the residual displacements are stable when the various parameters in the particular correction scheme are varied. We find that in many (but not all) cases the displacements are too sensitive to the parameters used in making the corrections for the residual displacements to be trusted. It is our opinion that low-cut filtering is usually needed, and in fact is often all that is needed, to obtain realistic-looking displacement time series. Although ground-displacement waveforms and peak motions can be sensitive to the type of correction, we find that the response spectra at periods of most engineering interest usually are not sensitive to the specific correction. Also, simple corrections to the digitally recorded accelerations often yield good estimates of ground motions at periods at least comparable to the duration of rupture, and therefore the corrected recordings are useful for modeling fault rupture.

Most of the data in this largely empirical study are from the **M** 7.1 1999 Hector Mine earthquake. We show that with simple processing the displacement waveforms for this event are very similar for stations separated by as much as 20 km.

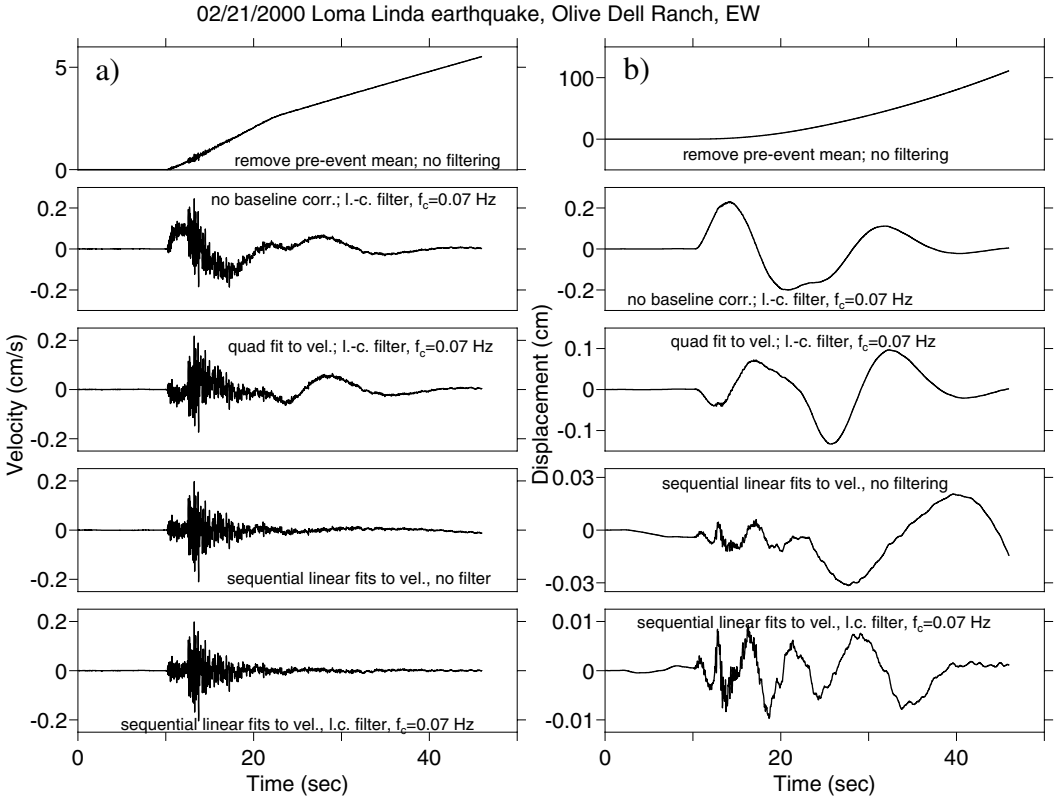

Figure 20. (a) Velocities and (b) displacements from various processing schemes applied to the acceleration time series shown in the bottom trace of Fig. 3a. The earthquake producing the ground motion was much smaller than the Hector Mine earthquake (M_L 4.4, compared with **M** 7.1). "l.c." stands for "low-cut."

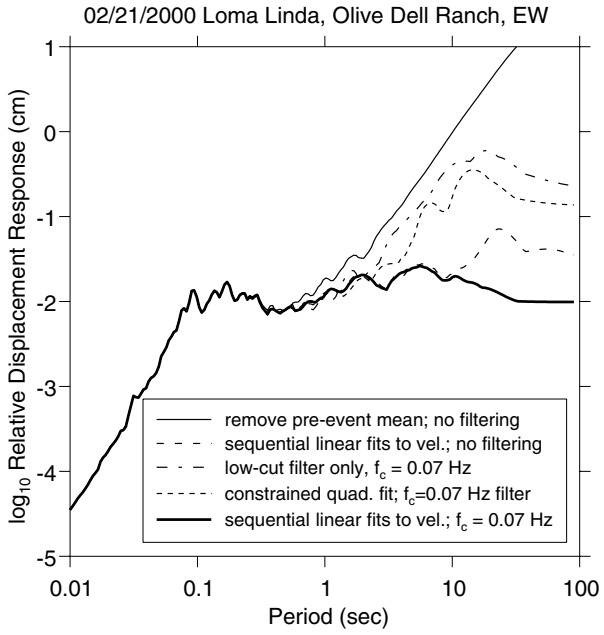

Figure 21. Five-percent-damped relative-displacement response spectra from the accelerations processed as in Fig. 20.

Although this was not a prime focus of the study, we find that a large pulse of SH energy with duration around 10 sec radiated from this earthquake, leading to velocity-response spectra that exhibit a pronounced peak at about 10-sec period.

Acknowledgments

We thank Dave Wald for a number of things, including providing a copy of Ji *et al.* in advance of publication, answering questions about the HEC recording, obtaining InSAR analysis from Y. Fialko, and reviewing the manuscript. We also thank many other individuals, including Yuri Fialko for his analysis of the InSAR data, Linda Seekins for providing data for HEC, Mehmet Celebi for information about the recording at station 699, Vladimir Graizer for communications regarding baseline corrections, Frank Scherbaum for checking our low-cut filter subroutine, and John Douglas for making us realize the importance of using double precision in response spectral computations for long oscillator periods. Hsi-Ping Liu, Mike Rymer, and Walt Silva provided useful reviews of the manuscript.

References

Abrahamson, N. A., and K. M. Shedlock (1997). Overview, *Seism. Res. Lett.* **68,** 9–23.

Abrahamson, N. A., and W. J. Silva (1997). Empirical response spectral attenuation relations for shallow crustal earthquakes, *Seism. Res. Lett.* **68,** 94–127.

Bommer, J. J., and A. S. Elnashai (1999). Displacement spectra for seismic design, *J. Earthq. Eng.* **3,** 1–32.

Boore, D. M. (1999). Effect of baseline corrections on response spectra for two recordings of the 1999 Chi-Chi, Taiwan, earthquake, *U.S. Geol. Surv. Open-File Rept. 99–545*, 37 pp.

Boore, D. M. (2001). Effect of baseline corrections on displacements and response spectra for several recordings of the 1999 Chi-Chi, Taiwan, earthquake, *Bull. Seism. Soc. Am.* **91,** 1199–1211.

Bradner, H., and M. Reichle (1973). Some methods for determining acceleration and tilt by use of pendulums and accelerometers, *Bull. Seism. Soc. Am.* **63,** 1–7.

Building Seismic Safety Council (BSSC) (1998). NEHRP recommended provisions for seismic regulations for new buildings and other structures, 1997 edition, Part 1: Provisions, prepared by the Building Seismic Safety Council for the Federal Emergency Management Agency (Rept. No. FEMA 302), Washington, D.C., 337 pp.

Chiu, H.-C. (1997). Stable baseline correction of digital strong-motion data, *Bull. Seism. Soc. Am.* **87,** 932–944.

Fialko, Y., and M. Simons (2001). The complete (3-D) surface displacement field in the epicentral area of the 1999 M_w 7.1 Hector Mine earthquake, California, from space geodetic observations, *Geophys. Res. Lett.* **28,** 3063–3066.

Graizer, V. M. (1979). Determination of the true ground displacement by using strong motion records, *Izv. Phys. Solid Earth* **15,** 875–885.

Graizer, V., A. Shakal, C. Scrivner, E. Hauksson, J. Polet, and L. Jones (2002). TriNet strong-motion data from the *M* 7.1 Hector Mine, California, earthquake of 16 October 1999, *Bull. Seism. Soc. Am.* **92,** 1525–1542 (this issue).

Hanks, T. C. (1975). Strong ground motion of the San Fernando, California, earthquake: ground displacements, *Bull. Seism. Soc. Am.* **65,** 193–225.

Huang, M. J., T. Q. Cao, D. L. Parke, and A. F. Shakal (1989). Processed strong-motion data from the Whittier, California, earthquake of 1 October 1987. I. Ground-response records, Rep. OSMS 89–03, California Strong Motion Instrumentation Program, Office of Strong Motion Studies, Division of Mines and Geology, California Dept. of Conservation, Sacramento, 175 pp.

Iwan, W. D., M. A. Moser, and C.-Y. Peng (1985). Some observations on strong-motion earthquake measurement using a digital accelerograph, *Bull. Seism. Soc. Am.* **75,** 1225–1246.

Ji, C., D. J. Wald, and D. V. Helmberger (2002). Source description of the 1999 Hector Mine, California, earthquake. II. Complexity of slip history, *Bull. Seism. Soc. Am.* **92,** 1208–1226 (this issue).

Lee, V. W., and M. D. Trifunac (1984). Current developments in data processing of strong motion accelerograms, Rept. 84–01, Dept. of Civil Engineering, Univ. of Southern California, Los Angeles, 99 pp.

Schiff, A., and J. L. Bogdanoff (1967). Analysis of current methods of interpreting strong-motion accelerograms, *Bull. Seism. Soc. Am.* **57,** 857–874.

Shakal, A. F., and C. D. Petersen (2001). Acceleration offsets in some FBA's during earthquake shaking (abstract), *Seism. Res. Lett.* **72,** 233.

Trifunac, M. D., and M. I. Todorovska (2001). A note on the useable dynamic range of accelerographs recording translation, *Soil Dyn. Earthq. Eng.* **21,** 275–286.

Wald, D. J., V. Quitoriano, T. H. Heaton, H. Kanamori, C. W. Scrivner, and C. B. Worden (1999). TriNet "ShakeMaps": Rapid generation of instrumental ground motion and intensity maps for earthquakes in southern California, *Earthq. Spectra* **15,** 537–556.

Appendix

Effect of Random Errors in Acceleration on Derived Displacements

Assume that the digital acceleration time series with time spacing Δt comprises random, uncorrelated noise having zero mean and a standard deviation σ_a. Velocity at time $t_k = (k - 1)\Delta t$ then can be approximated by

$$v(t_k) = \sum_{i=1}^{k} a(t_i)\Delta t. \tag{A1}$$

(This formula ignores the values of 0.5 for the first and last points for trapezoidal integration; the analysis here has been done for the more exact integration formula, but for the number of digital points of interest, the results are the same.) This equation expresses a classic random-walk stochastic process. Integration to displacement can then be approximated by

$$d(t_N) = \sum_{k=1}^{N} v(t_k)\Delta t. \tag{A2}$$

Combining the two summations and then grouping the coefficients of each acceleration term $a(t_i)$ yields the following equation:

$$d(t_N) = \sum_{i=1}^{N} (N - i + 1)a(t_i)\Delta t^2. \tag{A3}$$

We now assume that $d(t_N)$ represents the final displacement (i.e., t_N is the duration of the record). The final displacement is a weighted sum of the digital acceleration values; it is a random variable linearly related to the random accelerations. In any realization of the process, the displacement will have a final value that may be less than or greater than zero. Because the mean of the accelerations are equal to zero, however, it is easy to see from equation (A3) that the expected mean of the final values also will be zero. Of more interest is the standard deviation of the final displacement, for this will provide insight into how large the final displacement might be if a random sample were drawn from the process (as basically occurs when a real record has been processed). Because the random variables $a(t_i)$ are assumed to be independent and are characterized by a Gaussian distribution with standard deviation σ_a, the variance of $d(t_N)$ is the sum of the variance of the accelerations, weighted by the coefficients in the sum in equation (A3). The expression for the variance contains the sum over i, which can be evaluated by replacing the sum with an integral. Doing this gives the following equation for the standard deviation of the final displacement:

$$\sigma_{d_N} = \left(\frac{T^3 \Delta t}{3}\right)^{1/2} \sigma_{a,} \tag{A4}$$

where $T = N\Delta t$ is the duration of the record. Using a more accurate representation of the relation between displacement and acceleration, Schiff and Bogdanoff (1967) give an expression equal to equation (A4) multiplied by 1.12.

Pre-event portions of many of the records used in this study were used to obtain values of σ_a. The values ranged from 0.06 cm/sec^2 for the T129 recording of the Chi-Chi, Taiwan, earthquake to 0.0023 cm/sec^2 for the HEC recording of the Hector Mine, California, earthquake. Plugging these values into equation (A4) with the appropriate values of Δt (0.005 sec for all but the HEC recording, for which it is 0.01 sec) and duration gives $\sigma_{d_N} = 2$ cm for the worst case (the Chi-Chi earthquake) and approximately $\sigma_{d_N} = 0.1$ cm for the other examples considered in this article. (Monte Carlo simulations gave similar values, confirming that equation A3 is correct.) Recalling that this analysis applies to unfiltered records, it is clear that these values are much smaller than the final displacements obtained by double integration of the uncorrected accelerations. For this reason, it is unlikely that the drifts observed in the displacements are related to simple accumulation of random error.

U.S. Geological Survey, MS 977
345 Middlefield Road
Menlo Park, CA 94025
boore@usgs.gov
cdstephens@usgs.gov

Manuscript received 5 February 2001.